Published online 3 February 2011 *Nucleic Acids Research, 2011, Vol. 39, No. 10* ***4315–4329***
doi:10.1093/nar/gkr049

The MobM relaxase domain of plasmid pMV158: thermal stability and activity upon Mn^{2+} and specific DNA binding

Fabián Lorenzo-Díaz[1], Lubomir Dostál[2], Miquel Coll[3,4], Joel F. Schildbach[2], Margarita Menéndez[5,*] and Manuel Espinosa[1,*]

[1]Centro de Investigaciones Biológicas, CSIC, Ramiro de Maeztu 9, 28040 Madrid, Spain, [2]Department of Biology, Johns Hopkins University, 3400 North Charles Street, Baltimore, MD 21218, USA, [3]Institut de Biología Molecular de Barcelona, CSIC, [4]Institute for Research in Biomedicine, Barcelona Science Park, Baldiri Reixac 10, 08028 Barcelona and [5]Instituto de Química Física Rocasolano, CSIC and CIBER of Respiratory Diseases (CIBERES), Serrano 119, 28006 Madrid, Spain

Received July 8, 2010; Revised January 17, 2011; Accepted January 18, 2011

ABSTRACT

Protein MobM, the relaxase involved in conjugative transfer of the streptococcal plasmid pMV158, is the prototype of the MOB_V superfamily of relaxases. To characterize the DNA-binding and nicking domain of MobM, a truncated version of the protein (MobMN199) encompassing its N-terminal region was designed and the protein was purified. MobMN199 was monomeric in contrast to the dimeric form of the full-length protein, but it kept its nicking activity on pMV158 DNA. The optimal relaxase activity was dependent on Mn^{2+} or Mg^{2+} cations in a dosage-dependent manner. However, whereas Mn^{2+} strongly stabilized MobMN199 against thermal denaturation, no protective effect was observed for Mg^{2+}. Furthermore, MobMN199 exhibited a high affinity binding for Mn^{2+} but not for Mg^{2+}. We also examined the binding-specificity and affinity of MobMN199 for several substrates of single-stranded DNA encompassing the pMV158 origin of transfer (*oriT*). The minimal *oriT* was delimited to a stretch of 26 nt which included an inverted repeat located eight bases upstream of the nick site. The structure of MobMN199 was strongly stabilized by binding to the defined target DNA, indicating the formation of a tight protein–DNA complex. We demonstrate that the *oriT* recognition by MobMN199 was highly specific and suggest that this protein most probably employs Mn^{2+} during pMV158 transfer.

INTRODUCTION

Bacterial plasmids are able to disseminate multiple resistance genes by conjugation. This horizontal gene transfer (HGT) is relevant because of the increase in infectious diseases provoked by dissemination of antibiotic-resistant bacterial pathogens (1,2). Among them, the Gram-positive (G+) bacterium *Streptococcus pneumoniae* (the pneumococcus) is responsible for nearly 2 000 000 human deaths annually, and this figure represents only 15–20% of the people infected (3). Thus, understanding HGT in pneumococcus and related bacteria may help in controlling the spread of medically important antibiotic resistance (4).

Conjugation between Gram-negative (G−) bacteria is a well-characterized HGT process (5). The mechanism involves the assembly of a stable multi-protein complex (the relaxosome) on a plasmid region termed origin of transfer (*oriT*), and the key player is a plasmid-encoded nicking-closing enzyme, the DNA relaxase (5). Initiation of transfer requires cleavage of the phosphodiester bond at a specific position within the *oriT* (the nick site) mediated by a Tyr residue of the relaxase, so that a covalent tyrosinyl-DNA adduct is formed (6,7). The cleaving reaction requires the target DNA to be in single-stranded configuration (ssDNA). Thus, like almost all cation-dependent nucleotidyl-transferase enzymes, relaxases leave a free 3′-OH end while remaining bound to the 5′-phosphate product. This complex is actively pumped to the recipient cell by a plasmid-encoded coupling protein and the transferosome, a type IV secretion system (8,9). Once in the recipient, the relaxase–ssDNA intermediate restores the original circular plasmid molecule after termination of transfer by means

*To whom correspondence should be addressed. Tel: +34 918 373 112 (extn 4209); Fax: +34 915 360 432; Email: mespinosa@cib.csic.es
Correspondence may also be addressed to Margarita Menéndez. Tel: +34 915 619 400 (extn 1326); Fax: +34 915 642 431; Email: mmenendez@iqfr.csic.es

of a reversion of the strand transfer reaction. Consequently, termination of DNA transfer resembles termination of rolling circle replication (RCR) (10). Finally, conversion of ssDNA molecules into double-stranded (ds) plasmids in the recipient cells is carried out by conjugative replication (11,12). Whereas self-transmissible plasmids encode the entire machinery for their transfer, many small plasmids only harbour an *oriT* and the relaxase gene (13,14). This second group, known as mobilizable plasmids, can be transferred when they co-reside in the cell with an auxiliary self-transmissible element that supply the coupling protein and the transferosome (14).

In spite of the knowledge accumulated during the past years on the structure and function of conjugative relaxases encoded by plasmids of G-bacteria (8), information on equivalent proteins encoded by plasmids from G+ bacteria is still scarce and limited to a small number of proteins, such as TraA_pIP501 (15,16), Mob proteins of pC221 (17,18) and MobM, encoded by the mobilizable plasmid pMV158 (19,20). In general, the C-terminal moiety of relaxases contains a DNA-helicase or primase domain and/or other functions related to membrane association and to protein–protein interactions, whereas the N-terminal moiety harbours the endonuclease (DNA nicking and closing) and DNA-binding domain. In many cases, the endonuclease domain exhibits, apart from the catalytic Tyr residue, a His-triad termed '3H motif' ($HxDx_4HuH$, with 'x' being any residue and 'u' a hydrophobic residue) which is involved in the coordination of a single divalent cation required for DNA cleavage (21). In the architecture of the N-terminal nuclease domains of the four conjugative relaxases whose structures have been solved, this cation was shown to be Mg^{2+} or Mn^{2+} in TraI_F (6), Ni^{2+}, Cu^{2+}, or Zn^{2+} in TrwC_R388 (7), and Mn^{2+} in MobA_R1162 (22) and TraI_pCU1 (23).

With respect to the DNA-binding activity, it has been demonstrated that the interactions between the relaxase and the *oriT* are sequence- and structure-specific. Plasmid *oriT*s are complex DNA regions that contain inverted repeats (IR) and A+T-rich tracts. In the plasmids R388 and F, both belonging to MOB_F family (24), an IR is located 8 and 9 bp upstream to the nick site, respectively. Binding analyses using different fluorescently-labelled DNA fragments suggested that the relaxase domain of TraI_F could bind to its *oriT* in two distinct manners with different sequence specificities (25). Nevertheless, *in vitro* TraI protein-binding affinities for several ssDNA mutants and *in vivo* transfer efficiencies of F plasmid derivatives did not always correlate (26). These latter results suggest that the essential function of some bases in the *oriT* may be to position the scissile phosphate bond for cleavage, rather than to directly contribute to binding affinity. In the TrwC relaxase-ssDNA structure, the IR forms a hairpin and several protein–DNA contacts are established (7). This conformation was reported to be important for the termination reaction in the recipient cell (27,28).

The MobM protein has been considered representative of a family of relaxases termed MOB_V, which encompasses nearly 100 members (24). However, little information on biochemical and structural parameters of MOB_V relaxases has been provided. For that reason, the objective of this work was to characterize the N-terminal relaxase domain of protein MobM. Full length MobM has 494 residues. We have cloned a region of the *mobM* gene encoding the first 199 N-terminal residues (MobMN199). MobMN199 was purified as a native protein using a new protocol involving an affinity chromatography followed by a gel filtration step. In contrast to the dimeric form of the full length protein, the purified MobMN199 was a monomer in solution, but kept its nicking activity on supercoiled pMV158 DNA. Its secondary structure was determined and thermal denaturation studies showed that structural stability of MobMN199 strongly depended on Mn^{2+} and on DNA binding. Although Mg^{2+} ions could replace Mn^{2+} for DNA cleavage, the former did not stabilize the MobMN199 structure, at least in the absence of its DNA substrate. MobMN199 binding affinities for Mn^{2+} and for several oligonucleotides containing the *oriT* sequence were also measured. The ssDNA-binding experiments allowed us to define a minimal *oriT* sequence that contains an IR upstream the nick site. The results presented here demonstrate that the *oriT* recognition by the MobM relaxase is highly specific and suggest that this protein most probably employs Mn^{2+} during pMV158 plasmid transfer.

MATERIALS AND METHODS

Bacterial strains, plasmids and oligonucleotides

Escherichia coli strains were grown on TY (Pronadisa, Spain) medium supplemented with 30 μg/ml kanamycin or 100 μg/ml ampicillin. *E. coli* BL21(DE3) was used for expression of MobM and MobMN199. The plasmid used for controlled MobM expression was pLGM2 (based on pET5 vector) (20). Plasmid used for cloning the *mobM* variant *mobMN199* was pET24(b) (Novagen). Purified pMV158 DNA was prepared from the *S. pneumoniae* 708 strain (29) by two consecutive CsCl gradients as described (30).

Oligonucleotides used for binding studies were synthesized and HPLC-purified by the Integrated DNA Technologies (Coralville, IA, USA): ORIT 42-mer GCA CACACTTTATGAATATAAAGTATAGTGTG/TTAT ACTTTA; IR1 18-mer ACTTTATGAATATAAAGT; IR2 24-mer TAAAGTATAGTGTG/TTATACTTTA; IR3 32-mer GCACACACTTTATGAATATAAAGTAT AGTGTG/; IR1+8 26-mer ACTTTATGAATATAAAG TATAGTGTG/; IR1-R 11-mer GAATATAAAGT; IR3-L 15-mer GCACACACTTTATGA; IR3-R 15-mer ATAAAGTATAGTGTG/; 10-NIC 10-mer GTATAGT GTG/, where '/' denotes the *oriT* nick site. The IR3, IR2 and ORIT oligonucleotides were also purchased with the Cy5 fluorophore label.

DNA amplification and cloning

To obtain plasmid pMobMN199, a 630-bp fragment that encodes the first 199 residues of MobM protein was amplified by PCR on pMV158 DNA (accession number X15669) with the following primers: NdeI-F (5′-AAGGA

GGGAAACATATGAGTTACA-3′; coordinates 3718–3741) and XhoI-R/STOP (5′-GAAGTTCCTCCTCGAG TTACATATCAGCCA-3′; coordinates 4347–4318). To facilitate cloning, forward and reverse primers included changes (underlined) to generate recognitions sites for *Nde*I and *Xho*I restriction enzymes, respectively. Furthermore, a single change (boldface) was also introduced in the reverse primer to get an *ochre* stop codon instead of Glu200 (E200Stop). PCR amplifications were done in 50-µl reaction mixtures containing reaction buffer 1× [16 mM $(NH_4)_2SO_4$, 67 mM Tris–HCl (pH 8.8), 1.5 mM $MgCl_2$], 0.2 mM of each dNTP (Roche), 0.4 µM of each primer, 0.65 U of Phusion DNA polymerase (Finnzymes) and 1 ng of DNA template, under the following conditions: an initial denaturing step at 98°C (30 s); 30 cycles of denaturation at 98°C (10 s), annealing at 55°C (20 s) and extension at 72°C (30 s) followed by a final extension at 72°C (10 min). PCR products were purified with the QIAquick gel extraction kit (Qiagen) and after digestion with *Nde*I and *Xho*I enzymes, the fragments were ligated into pET24(b) previously digested with the same enzymes. The constructs were confirmed by nucleotide sequencing. *Escherichia coli* BL21(DE3) cells harbouring the desired plasmid were used for protein expression.

Protein purification and N-terminal sequencing

MobM and MobMN199 proteins were overproduced and purified by a newly developed protocol, with greater speed and higher yield than the one previously described for MobM (19,20). Briefly, cells were grown in 4 l of TY-Km at 37°C to reach an OD_{600} = 0.5. Expression of the plasmid-encoded genes was achieved by induction with 1 mM IPTG (30 min), followed by addition of rifampicin (200 µg/ml) and growth for an additional 90 min. Cells were sedimented by centrifugation (8000 rpm, 20 min, 4°C) and stored at −80°C. The cell pellet was thawed and resuspended (100× concentrated) in buffer A [20 mM Tris–HCl pH 7.6, 1 mM EDTA, 1 mM dithiothreitol, 5% (v/v) glycerol] plus 1 M NaCl and a tablet of protease inhibitor cocktail (Complete, Roche). Cells were then lysed by passage through a French pressure cell and the extract was centrifuged to remove cell debris. The clarified extract was treated with 0.2% (v/v) polyethyleneimine (Sigma) to precipitate nucleic acids, and proteins in the supernatant were precipitated at 70% (w/v) ammonium sulphate saturation. The proteins in the precipitate were collected by centrifugation and dissolved in buffer A with 300 mM NaCl. After equilibration in the same buffer by dialysis, the sample was loaded onto a 100 ml heparin–agarose (BioRad) column (flow rate of 50 ml/h). After washing with 5-column volumes of the same buffer, a 400 ml 0.3–0.8 M NaCl gradient was applied to elute the proteins retained. Fractions were analysed by 15% SDS–Tris–glycine polyacrylamide (PAA) gel electrophoresis followed by staining with Bio-safe Coomassie (BioRad Laboratories). Fractions containing the peak of MobMN199 were pooled, dialysed against buffer A containing 500 mM NaCl, and concentrated by filtering through 3 kDa cut-off membranes (Pall) until the sample volume reached 1 ml. The protein sample was injected at 0.5 ml/min onto a HiLoad Superdex 200 gel-filtration column (Amersham) and subjected to fast-pressure liquid chromatography (FPLC; Biologic DuoFlow from BioRad). OD_{280} values were monitored continuously and each recovered fraction (2 ml) was analysed as above. Fractions containing pure MobMN199 protein (>98%) were pooled and concentrated until the final concentration was 5 mg/ml protein and stored at −80°C. In these conditions, the protein retained full activity for at least 1 year. Edman's sequential degradation was applied to analyse the N-terminal sequence of MobMN199 in a Procise 494 protein sequencer (Perkin Elmer) as reported (20). Concentration of MobMN199 protein was determined by spectrophotometric determinations and by determination of the amino acid composition of the protein (CIB-Protein Chemistry Service).

Supercoiled DNA relaxation assays

Nicking of supercoiled DNA by purified MobM or MobMN199 was performed essentially as reported (20). Standard reaction mixtures (20 µl) contained supercoiled pMV158 DNA (300 ng) in buffer N [20 mM Tris–HCl pH 7.6, 200 mM NaCl, 0.05 mM EDTA, 1% (w/v) glycerol, 1 mM dithiothreitol] to which different concentrations of divalent cations and purified protein were added. Samples were incubated at 30°C for 20 min, and reactions were stopped by addition of SDS (0.5%) and Proteinase K (100 µg/ml), followed by 30 min incubation. Generation of open circular forms (FII) by the nicking activity of MobMN199 was monitored by electrophoresis on 1.2% (w/v) agarose gels and quantified as described (20).

Analytical ultracentrifugation

Sedimentation equilibrium experiments were performed at 20°C in an Optima XL-A (Beckman-Coulter) analytical ultracentrifuge. A range of MobMN199 concentrations, from 2 to 20 µM protein, were examined in buffer UA [20 mM Tris–HCl pH 7.6, 500 mM NaCl, 1 mM EDTA, 1% (v/v) glycerol]. Samples (100 µl) were centrifuged at two successive velocities (20 000 and 35 000 rpm) and absorbance was measured at 3 h intervals to determine that samples had reached equilibrium. The equilibrium scans were monitored at the most appropriate wavelength (230, 280 or 290 nm), depending upon the MobMN199 concentration employed. Baseline signals were measured after high-speed centrifugation. Apparent average molecular masses ($M_{w,app}$) of MobMN199 were obtained using the program Heteroanalysis (www.biotech.uconn.edu). The partial specific volume of MobMN199, 0.723 ml/g, was calculated from its amino acid composition with the programme SEDNTERP (31). Sedimentation velocity experiments were performed at 48 000 rpm and 20°C with 400 µl samples of MobMN199 (2–20 µM, in buffer UA) that were loaded into double-sector cells. The sedimentation coefficient distribution for MobMN199 was calculated by least-squares boundary modelling of sedimentation velocity data using the sedimentation coefficient distribution method, as implemented in the SEDFIT program (32). The coefficient was corrected to standard conditions to get the corresponding $s_{20,w}$ value using the SEDNTERP

program. The translational frictional coefficient of MobMN199 (f) was determined from the molecular mass and sedimentation coefficient of the protein (33), whereas the frictional coefficient of the equivalent hydrated sphere (f_0) was estimated using a hydration of 0.4506 g H_2O per g protein (34).

Sequence-based secondary structure prediction

Secondary-structure predictions of MobMN199 were carried out with programs PSIPRED (35), Jpred (36), SABLE (37), NPS@ (38) and PredictProtein (39) (http://www.expasy.ch/). The average number of residues involved in alpha helix, extended strand or random coil was calculated, and a secondary structure model of MobMN199 was constructed.

Circular dichroism

CD spectra were acquired from 185 to 260 nm in a J-710 spectropolarimeter (Jasco Corp.) fitted with a Peltier temperature control accessory using 0.02–0.1 cm optical path length quartz cells. Each spectrum was the average of four cumulative measurements, performed automatically, that were recorded at a scanning speed of 20 nm/min and 1 nm spectral bandwidth. Measurements were performed at 15 μM MobMN199 and the spectra were corrected by subtracting the buffer contribution. To obtain structural information, spectra were acquired at 10°C in buffer CD1 (20 mM sodium phosphate, pH 7.6, 50 mM ammonium sulphate), converted to mean residue ellipticity ($[\Theta]_{MRW}$) or to differences in molar absorbance ($\Delta\varepsilon$) and then deconvolved using CONTINLL (40) and SELCON3 (41) algorithms, with the reference data set #6, available at DichroWeb site (42). To analyse the temperature-associated changes in secondary structure with different Mn^{2+} or Mg^{2+} concentrations ('Results' section), MobMN199 was dialysed against buffer CD2 (20 mM HEPES pH 7.6, 50 mM ammonium sulphate), unless otherwise stated, and changes in ellipticity at 218 nm were recorded in 0.1 cm optical path-length quartz cells while increasing the temperature from 10 to 90°C at two different rates (20 and 50°C/h). In addition, CD spectra obtained from 205 to 260 nm were recorded between 10 and 90°C with temperature increments of 5°C and equilibration times of 1 min before acquiring each spectrum. Finally, the sample was cooled again to the initial temperature (10°C) and the protein spectrum was recorded under renaturing conditions. Data acquisition and processing were carried out using the Jasco Spectra-Manager software, and thermal-denaturation profiles were analysed in terms of two two-state transitions [Equation (1)] using the Origin v6.0 software (Microcal Inc.):

$$\Delta\Theta(T)/\Delta\Theta_{max} = \sum_{i=1}^{2} f_i \frac{\{\exp[-\Delta H_i(T_{mi}-T)/R\times T_{mi}\times T]\}}{\{1+\exp[-\Delta H_i(T_{mi}-T)/R\times T_{mi}\times T]\}}, \quad (1)$$

where $\Delta\Theta(T)$ is the ellipticity change at 218 nm at temperature T, $\Delta\Theta_{max}$ the maximum variation in the ellipticity at this wavelength, R the gas constant, f_i the relative contribution of transition i to $\Delta\Theta_{max}$, and T_{mi} and ΔH_i are the half-transition temperature and the enthalpy change of this transition, respectively.

Calorimetric studies

Isothermal titration calorimetry (ITC) was performed using a MicroCal MCS-ITC calorimeter (Microcal Inc.). Before measurements, MobMN199 samples were dialysed against buffer ITC (20 mM HEPES, 400 mM NaCl, pH 7.6), which was also used to prepare the cation solutions. The protein was loaded into the calorimetric cell at a concentration of 75 μM and titrated by stepwise injection of 1.5 mM $MnCl_2$ or 20 mM $MgCl_2$ solutions. Typically, twenty 3–8 μl injections were performed while stirring at 300 rpm, and the heat of the dilution of the ligand was determined in separate runs. The experiments were carried out at 17°C and the binding isotherms were analysed using the Microcal Origin ITC software package. Differential scanning calorimetry (DSC) measurements were performed at a heating rate of 50°C/h in a VP-DSC microcalorimeter (Microcal Inc.), at a constant pressure of 2 atm. MobMN199 was equilibrated in ITC buffer supplemented with the required Mn^{2+} concentration. Experiments performed in the presence of DNA (oligonucleotide IR1+8) were carried out at a MobMN199/DNA ratio of 2.0 using protein concentrations of 40 and 20 μM. Microcal Origin DSC software was used for data acquisition and analysis. Excess heat capacity functions were obtained after subtraction of the buffer–buffer base line and transformed into molar heat capacities dividing by the number of moles of MobMN199 in the DSC cell.

DNA-binding affinity measurements

Titration of MobMN199 with 5′- or 3′-labelled (Cy5) oligonucleotides was performed by electrophoretic mobility shift assays (EMSA), as reported (43). Purified MobMN199 was mixed, at different concentrations, with Cy5-labelled DNA (2 nM) in 10 μl of buffer A with 300 mM NaCl. Reaction mixtures were incubated at 25°C for 30 min. Free and bound DNAs were separated by electrophoresis on native 10% PAA gels. Fluorescent DNA bands were detected with a Typhoon scanner system (Molecular Dynamics) and quantified with QuantityOne software (Bio-Rad). Competitive EMSA were used to determine the relative affinities of MobMN199 for different DNA sequences. Mixtures of Cy5′-IR3 oligonucleotide (2 nM) and DNA fragments at differing concentrations were incubated simultaneously with 80 nM MobMN199 protein. The samples were incubated at 25°C for 30 min, loaded on native 10% PAA gels and the DNA species were quantified as above.

RESULTS

Characterization of the MobM relaxase domain

The full-length MobM protein has a predicted size of 57 874 Da (494 residues) and exhibits three conserved

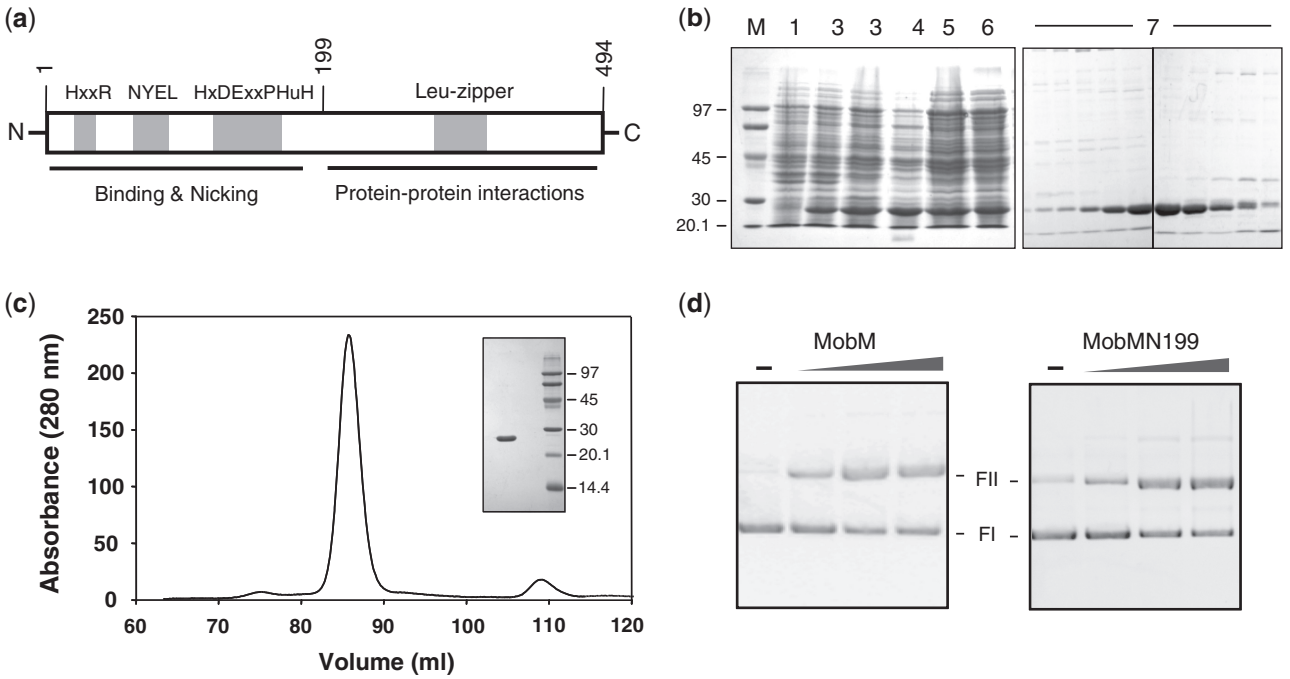

Figure 1. (**a**) Predicted domains in the native MobM protein. The three conserved motifs located in the N-terminal moiety are indicated: (i) HxxR (unknown function), (ii) NYEL (proposed catalytic region) and (iii) HxDExxPHuH (metal ion coordination). The position of the putative Leu zipper in the C-terminal moiety is also indicated. (**b**) Stages in the purification of MobMN199. Fractions of the different purification steps were analysed by electrophoresis on 15% SDS–Tris–glycine–PAA gels. Samples loaded were: uninduced cultures (lane 1); cultures induced with IPTG and rifampicin (lane 2); supernatant of a total cell lysate (lane 3); supernatant after PEI precipitation (lane 4); supernatant of the ammonium sulphate precipitation step before (lane 5) and after (lane 6) dialysis against buffer A. The sample was loaded onto a heparin–agarose column and the proteins retained were eluted by a salt gradient (covered by lane 7). Fractions containing the peak of MobMN199 were pooled, dialysed against buffer A and concentrated. M indicates the molecular weight standards (in kDa). (**c**) Purified MobMN199 was injected onto a gel filtration column, and its elution profile was recorded; the inset shows the SDS–PAGE gel with the purified protein and the molecular size markers. (**d**) Relaxation assays with wild-type MobM and the MobMN199 protein. Supercoiled pMV158 DNA samples (300 ng; 8 nM) were incubated with and without (−) full-length MobM (left) or with the short MobMN199 fragment (right) in the presence of 15 mM $MnCl_2$ at 30°C, 20 min. Protein concentrations used were 120, 240 and 480 nM. Generation of relaxed forms (FII) from supercoiled DNA forms (FI) was analysed by electrophoresis on 1% agarose gels without prior staining with EtBr, conditions in which forms FI′ are not resolved. The amounts of relaxed DNA forms generated by treatment of MobM and by MobMN199 were calculated by subtracting the amount of already nicked molecules (faint FII band in the untreated samples generated by mechanical shearing) from the FII-forms generated by protein treatment. The values of the protein-relaxed molecules were 25, 42 and 62%, and 28, 40 and 63% for samples treated with MobM and MobMN199, respectively. The weak band above relaxed forms FII has been observed before (20) and might correspond to relaxed DNA dimers.

motifs located in the N-terminal moiety (Figure 1a): (i) motif I (HxxR), of unknown function; (ii) motif II (NYD/EL), which contains the putative catalytic tyrosine; and (iii) motif III (HxDExxPHuH), also known as the 3H motif, probably involved in coordination of a divalent metal (13). To uncouple the N- and C-terminal domains of MobM, a strategy to obtain a protein containing only the first 199 N-terminal residues (MobMN199) was designed. The strategy was based on alignment of the relaxases belonging to the MOB_V family (24), of which pMV158 is the prototype, revealed that roughly the first 200 amino acids were highly conserved among all the relaxases. Inspection of the DNA sequence around this region indicated that generation of a stop codon after the first 199 residues was relatively simple. Thus, the 5′-region of the pMV158 *mobM* gene (encoding the first 199 residues followed by a stop codon) was cloned into a suitable expression vector. To purify MobMN199, the protocol employed to obtain the full-length MobM protein (19) was improved by introducing one step of precipitation with polyethyleneimine (to precipitate nucleic acids), followed by an affinity (heparin-agarose) chromatography, and a final gel-filtration chromatography step (Figure 1b and c, and Supplementary Table S1). This new procedure allowed us to scale up the purification, so that the final yield of the MobMN199 protein was ~4.5 mg/l of cell culture and purity was >98%. Under denaturing conditions, MobMN199 migrated between 30 and 20.1 kDa reference bands (Figure 1c), which agrees with the size of the protein predicted from its DNA sequence (23 261 Da; 199 residues). Determination of the N-terminal amino acid sequence showed that residue Met1 was removed, and the mass determined by MALDI-TOF (23 128 Da, not shown) was in agreement with the calculated molar mass (23 129 Da without Met1).

The ability of MobMN199 to convert supercoiled DNA (form FI) into open circular species (form FII) was tested at several protein concentrations (from 120 to 480 nM) and reactions were performed in the presence of 15 mM $MnCl_2$. The samples were incubated at 30°C for 20 min, as reported for the full-length protein (19,20). The results showed that MobMN199 was able to relax pMV158 DNA with the same efficiency as the entire MobM,

converting up to 60% of supercoiled plasmid into form FII (Figure 1d). The failure to reach 100% cleavage could be explained as the result of the equilibrium between the nicking and closing activities of MobMN199; a behaviour observed for several relaxases (44–46). Selective precipitation by KCl and SDS of FII forms cleaved by a relaxase is the procedure used to detect relaxosome formation (46). We have previously shown that the full-length MobM protein was able to form stable complexes with pMV158 DNA, most likely through a covalent linkage (20). Similar experiments performed with MobMN199 showed that the FII forms generated by the truncated protein were also precipitated by KCl and SDS (not shown). This result indicates that the N-terminal domain of MobM contains all the information needed to generate a relaxosome with its target DNA.

Analytical ultracentrifugation analyses showed that the entire MobM protein behaved as an elongated dimer in solution (19). Since the shorter version MobMN199 lacks the last 295 C-terminal amino acids, we wanted to determine its oligomeric state and hydrodynamic properties. The elution volume of the truncated protein in the size-exclusion chromatography used for purification (Figure 1c) suggested that MobMN199 was a monomer. To corroborate this, analytical ultracentrifugation assays were performed at three protein concentrations (2, 8 and 20 μM). The results of sedimentation equilibrium and velocity assays are shown in Figure 2. Sedimentation velocity profiles fit well to a model of single sedimenting species (98.1% of total concentration loaded), with an $s_{20,w}$ value of 2.37 S, and an average molecular mass ($M_{w,app}$) of 22 944 ± 2820 Da, which agrees with the monomer mass determined by MALDI-TOF. No improvement in the best-fitting parameters was obtained considering more sedimenting species, an indication of sample homogeneity. At 8 μM, the experimental sedimentation equilibrium data fitted best to a $M_{w,app}$ of 23 000 ± 700 Da, which agrees with the value obtained from the sedimentation velocity. Similar average molecular masses were determined when MobMN199 concentrations of 2 μM (22 637 Da) and 20 μM (21 985 Da) were used. The frictional ratio (f/f_0) calculated was 1.25, indicating that MobMN199 clearly deviates from the behaviour expected for globular particles ($f/f_0 \cong 1$). Moreover, since the results fit to the MobMN199 monomer mass, we can conclude that MobM dimerization requires the C-terminal portion of the protein, which should also comprise the protein dimerization domain. Plasmids bearing mutations that result in deletions of either the 18 or the 30 last codons of gene *mobM* failed to be transferred between pneumococci (our unpublished observations). In addition, mutations directed to a predicted coiled-coil region in MobM (19) also resulted in plasmids unable to be transferred. Based in all these results, we tentatively propose that the C-terminal moiety of MobM would be involved in other transactions during the transfer process, like dimerization, membrane association and interactions with the coupling protein which would be provided by the auxiliary plasmid.

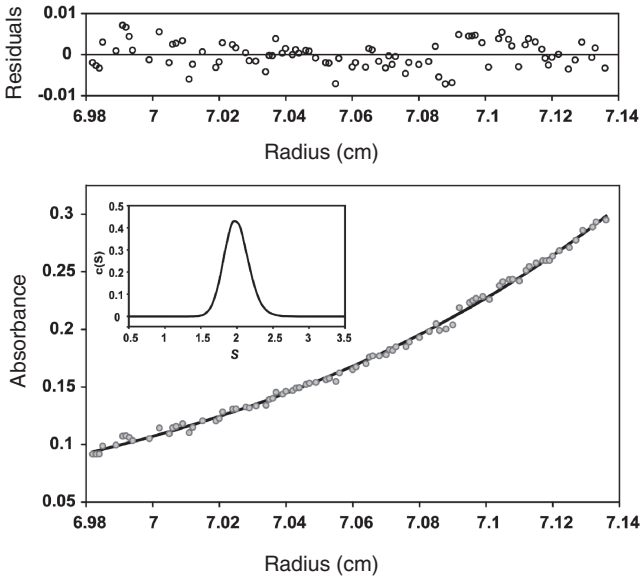

Figure 2. Sedimentation equilibrium profile of MobMN199 (8 μM of protein in buffer UA) at 35 000 rpm and 20°C (λ = 280 nm). The lower part shows the experimental data (circles) and the best fit (solid line) to a single species with M_w = 23 101 Da. The upper part shows residuals of the theoretical fit. The inset shows the distribution of sedimentation coefficients of the same MobMN199 protein sample in sedimentation velocity experiments (48 000 rpm, 20°C).

Secondary-structure content of MobMN199

The predicted secondary-structure of MobMN199 obtained by computational methods (Figure 3a) indicated a distribution of α-helices alternating with β-strands (the so-called α/β-fold), which is a typical feature of the Rep/Mob family of relaxases with known structures, including RepB_pMV158 (47), TraI_F (6), TrwC_R388 (7) and MobA_R1162 (22). The results were tested experimentally by CD in the far-UV region (Figure 3b). The CD spectrum of MobMN199 showed two minima at 208 and 222 nm, a characteristic feature of α-helical structures. Estimation of the secondary-structure yielded similar results when two different deconvolution methods were used (Table 1). The average of α-helices and β-strands content provided by these two methods agrees with the predicted secondary structure. The reduction of the total α-helical content (~40%) of MobMN199 as compared to the full-length protein (~60%) is consistent with the high content in α-helices predicted for the C-terminal moiety of the MobM protein (19).

Influence of Mn^{2+} on MobMN199 thermal stability

To determine the influence of Mn^{2+} and Mg^{2+} on MobMN199 structural stability, CD spectroscopic studies were performed in the absence or presence of either cation (Figure 4a). Changes in the ellipticity associated with protein denaturation were monitored at 218 nm while the temperature was increased from 10 to 90°C at the rate of 50°C/h or 20°C/h with similar results. Denaturation of the unbound protein started around 15°C (Figure 4a; black triangles). The ellipticity strongly decreased as the temperature was increased,

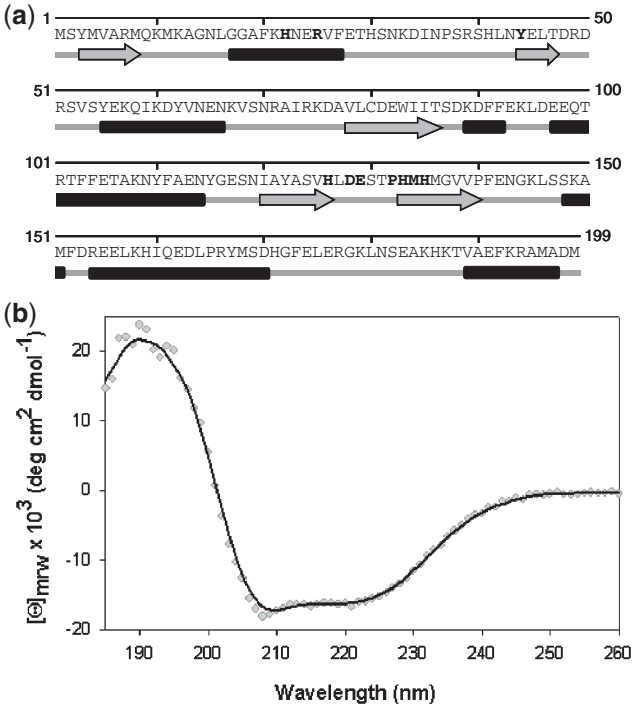

Figure 3. Secondary-structure analysis of MobMN199. (**a**) Computational analyses. The amino acid sequence of MobMN199 is depicted as well as a summary of the most reliable predictions of secondary structure (using PSIPred, Jpred, NPS@, SABLE and PredictProtein programs). Boxes and arrows below the amino acid sequence of MobMN199 correspond to helices and β-strands, respectively. Boldface letters indicate the conserved residues in the MobM family (Figure 1a). (**b**) CD spectra of MobMN199 (15 μM) protein in buffer CD1, at 10°C. The solid line represents the fit of the experimental curve by the CONTIN method. Experimental data (diamonds) were acquired using 0.02-cm optical path-length quartz cells.

Table 1. MobMN199 secondary-structure content

Method used	α-Helix	β-Strand	Turns	Unordered
Deconvolution				
CONTIN	41.1	14.8	20.2	24
SELCON3	47.4	7.9	22	24.1
Average	44 ± 4	11 ± 5	21 ± 1	24.0 ± 0.1
Prediction				
PSIPred	41.9	19.2	ND	38.9
Jpred	38.4	16.2	ND	45.5
NPS@	47.5	10.1	ND	42.4
SABLE	37.9	18.2	ND	43.9
PredictProtein	36.9	15.7	ND	47.5
Average	40 ± 4	16 ± 4		44 ± 3

Data and standard deviation are given in percentages. ND, not determined.

showing a denaturation profile that slightly deviated from the behaviour expected for a two-state transition (Figure 4). Addition of Mn^{2+} at one-to-one stoichiometry strongly modified MobMN199 denaturation, shifting the apparent transition temperature by ~5°C. A further increase in Mn^{2+} concentration clearly showed the presence of at least two different processes, particularly at the higher Mn^{2+} concentrations tested. A very different picture was observed when the cation used was Mg^{2+}: even at 15 mM, the metal concentration typically used in DNA-nicking assays (19), Mg^{2+} addition only induced a small thermal up-shift in the final part of the denaturation profile (Figure 4a; orange triangles).

The reversibility of MobMN199 denaturation was examined by recording the protein spectra after cooling the heated samples to the initial temperature of the experiments. Under renaturing conditions, the spectrum of the native protein was substantially recovered (Figure 4b), indicating that MobMN199 was able to refold, at least to a large extent (~60–70%), both in the absence and in the presence of added cations. In addition, the functionality of refolded MobMN199 samples was addressed by performing a cleavage assay on supercoiled pMV158 DNA (FI forms) at 30°C in the presence or absence of the two tested divalent cations. Activity assays showed that MobMN199 was active after the slow heating and cooling steps (Supplementary Figure S1). The specific appearance of open circle forms (FII) as well as relaxed covalently closed forms (FI′) demonstrated the nicking-closing activity of the refolded protein. Although the closing activity of MobMN199 samples renatured in the absence of cation was significantly lower (~16% FI′ forms) than the one shown by the native protein (~50% FI′ forms), it was almost completely restored when the protein refolded in buffers containing Mg^{2+} (33% FI′ forms) or Mn^{2+} (52% FI′ forms).

The analysis of the CD denaturation profiles showed that they could be described as the superimposition of two apparently independent processes whose thermodynamic parameters are summarized in Table 2. The values of their relative contributions to the total ellipticity change at 218 nm with and without Mn^{2+} could indicate that the first transition observed in the absence of metal cations ($F_i \sim 0.36$) would correspond to the highest temperature in Mn^{2+}-bound samples. The assumed model was further supported by the CD denaturation experiments carried out in ITC buffer (see below).

The influence of Mn^{2+} (and of DNA binding; see below) in MobMN199 structural stability was also examined by DSC. At 124 μM Mn^{2+} (Mn^{2+}:MobMN199 ratio 1.5), denaturation apparently takes place in a single step with an enthalpy change, ΔH_D, of 41 kcal/mol and a T_m of 45°C (Figure 5a), and can be described in terms of a two-state transition (red dashed line). However, the heat capacity profile was significantly affected by the cation concentration and, at 8 mM Mn^{2+}, MobMN199 denaturation proceeded with a substantial increase of the total enthalpy change ($\Delta H_D = 93$ kcal/mol). In addition, deconvolution of the endotherm indicated that, at this cation concentration, MobMN199 unfolding might take place in three steps (Figure 5a). The two first conform to the two-state transition model ($T_{mB1} = 43.1$°C, $\Delta H_{B1} = 34$ kcal/mol, $T_{mB2} = 50.2$°C, $\Delta H_{B2} = 55$ kcal/mol) and would take place, approximately, in the same temperature interval as the first step observed in the CD profile recorded at this cation concentration. In addition, the shoulder appearing at high temperature ($T_{mA} \cong 63$°C) might

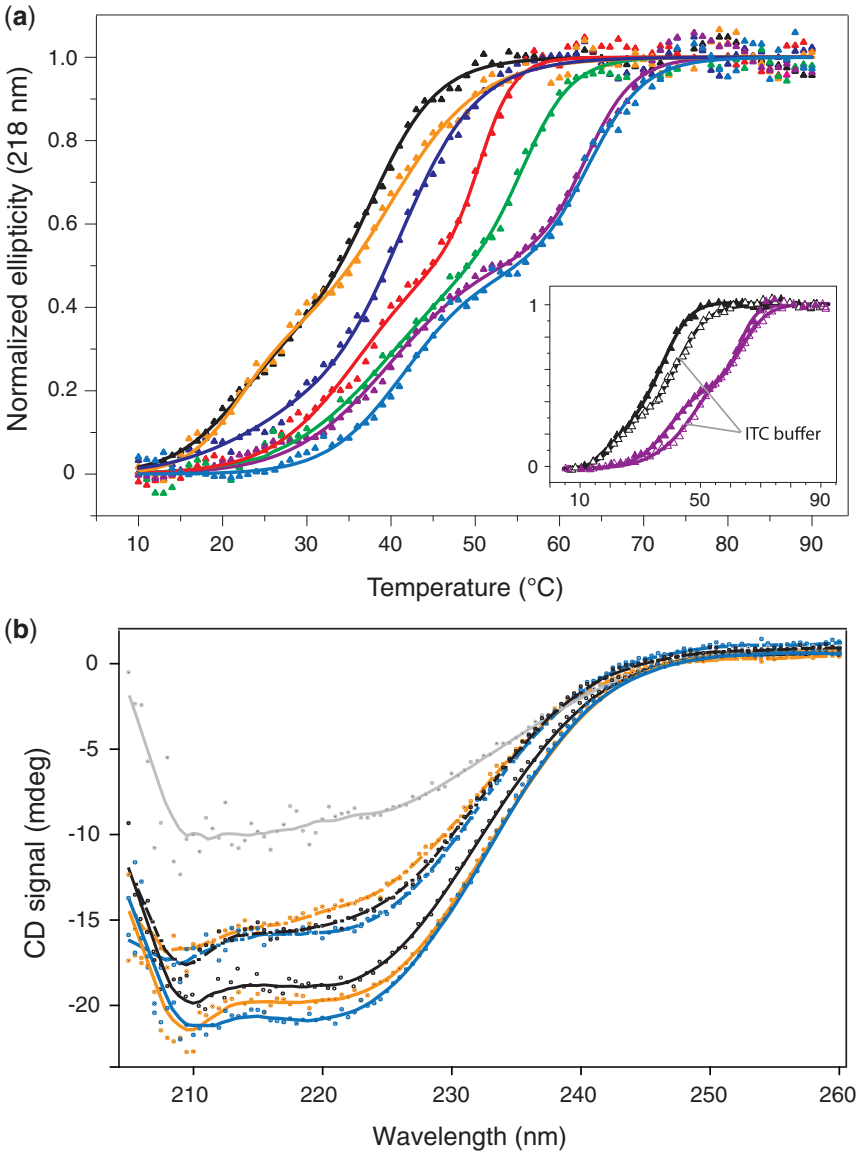

Figure 4. Temperature-associated changes in the secondary-structure of MobMN199. (**a**) Thermal denaturation profiles of the protein (15 µM) measured at 218 nm in presence or absence of divalent metals (free protein, black; 15 mM $MgCl_2$, orange; 0.015 mM $MnCl_2$, dark blue; 0.2 mM $MnCl_2$, red; 1.5 mM $MnCl_2$, green; 8 mM $MnCl_2$, purple; and 15 mM $MnCl_2$, blue). Data fit (continuous lines) assumed the superimposition of two apparently independent transitions whose thermodynamic parameters are shown in Table 2. The inset compares the thermal denaturation profiles of MobMN199 in CD2 (solid symbols) and ITC (open symbols) buffers in the absence (black) and in the presence (purple) of 8 mM $MnCl_2$. (**b**) Far-UV CD spectra registered before denaturation (10°C, solid lines) or under renaturing conditions (heated samples cooled to 10°C, dashed lines) without metal (black), and in the presence of 15 mM Mg^{2+} (orange) or 15 mM Mn^{2+} (blue). A spectrum of MobMN199 at 85°C (solid grey line) is also depicted.

correspond to the last step of CD curves (Figure 4a). As DSC studies were performed in the ITC buffer that contained NaCl instead of $(NH_4)_2SO_4$, the loss of secondary structure was also monitored in the former buffer following the ellipticity change at 218 nm. Substitution of ammonium sulphate by sodium chloride modified the thermal denaturation profile that became clearly biphasic, even in the absence of Mn^{2+} (Figure 4a, inset). Its deconvolution in terms of two two-state transitions showed an increase of about 5°C in the T_m value of the second transition (Table 2 and inset in Figure 4) whereas the first one remained unchanged. These observations support the analyses of the CD profiles monitored in the absence of Mn^{2+} and at low cation concentration in buffer CD2 in terms of two transitions. Moreover, the shift of both transitions to higher temperatures upon addition of 8 mM Mn^{2+} was comparable in both buffers (Table 2; inset Figure 4a). However, comparison of DSC and CD results suggested that the first process observed in CD denaturation profiles might actually comprise two transitions at high Mn^{2+} concentrations. Indeed, a better fit of the CD curve recorded at 8 mM Mn^{2+} in ITC buffer was obtained using the DSC-derived thermodynamic parameters (Table 2).

Table 2. Apparent thermodynamic parameters for MobMN199 CD thermal transitions

Buffer	$[MnCl_2]$[a]	T_{m1}	$\Delta H_{1,app}$	F_1	T_{m2}	$\Delta H_{2,app}$	F_2
CD2	NA	21 ± 2	44 ± 8	0.33 ± 0.07	37.8 ± 0.8	48 ± 4	0.67 ± 0.07
	0.2	37 ± 2	34 ± 5	0.6 ± 0.1	51.0 ± 0.6	110 ± 40	0.4 ± 0.1
	1.5	41 ± 3	30 ± 4	0.6 ± 0.1	55.8 ± 0.6	100 ± 40	0.4 ± 0.1
	8	42 ± 1	29 ± 2	0.60 ± 0.04	64.0 ± 0.4	87 ± 10	0.41 ± 0.04
	15	42 ± 1	52 ± 10	0.48 ± 0.06	63.5 ± 0.9	68 ± 15	0.52 ± 0.06
	15 (Mg^{2+})	22 ± 2	50 ± 20	0.3 ± 0.1	40 ± 2	37 ± 7	0.7 ± 0.1
ITC	NA	22 ± 1	44 ± 7	0.32 ± 0.04	42.8 ± 0.6	41 ± 3	0.68 ± 0.04
	8	46.5 ± 0.4	28 ± 2	0.6 ± 0.1	64.1 ± 0.6	48 ± 5	0.4 ± 0.1
		(43.1 ± 0.9)[b]	(34 ± 4)	(0.39 ± 0.02)	(65.1 ± 0.7)	(56 ± 7)	(0.43 ± 0.03)
		(50.2 ± 0.1)	(55 ± 1)	(0.18 ± 0.05)			

[a]Concentrations are given in millimolar units. Addition of Mg^{2+} instead Mn^{2+} is indicated.
[b]Data in parenthesis correspond to the fit based on DSC parameters (see Figure 5 and text for details).
NA, not added.

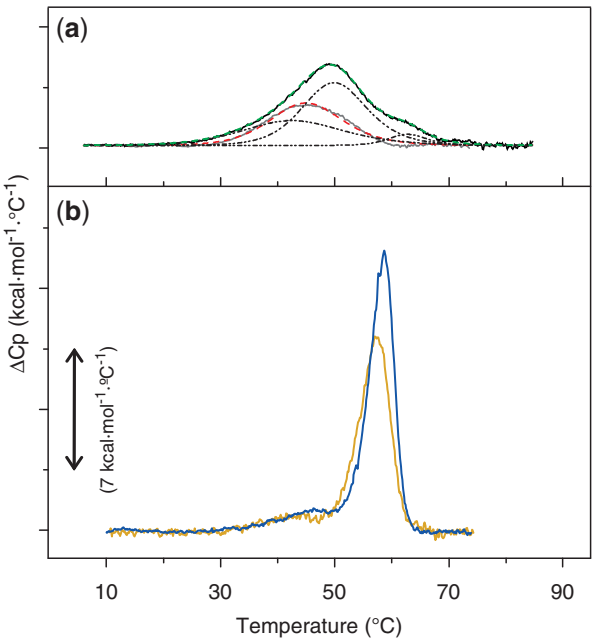

Figure 5. Thermal denaturation of MobMN199 relaxase measured by DSC. (**a**) Influence of Mn^{2+} binding. Continuous grey and black lines are the thermograms of DNA-free protein monitored at 124 µM and 8 mM Mn^{2+} (83 µM MobMN199), respectively. Dashed red line is the fit of MobMN199 thermogram at low Mn^{2+} concentration to the two-state model. Dashed–dotted black lines are the elementary transitions under the thermogram at 8 mM $MnCl_2$ assuming that MobMN199 denaturation takes place in three steps and the dashed–dotted green line is the theoretical envelope ('Results' section). (**b**) Influence of DNA binding. The presence of oligonucleotide IR1+8 shifted the unfolding endotherms of MobMN199 toward higher temperatures. Curves monitored at fixed protein:DNA ratio of 2:1 are in dark yellow (13.3 µM:6.5 µM) and blue (40 µM:20 µM). Mn^{2+} concentrations were fixed to have a free metal concentration of 82 µM at half denaturation.

MobMN199 affinity for cations

The affinity of MobMN199 for Mn^{2+} and Mg^{2+} was examined by ITC. Titrations were performed at 17°C to preserve the native state of MobMN199 during the experiment. The analysis of the binding isotherms (Figure 6) showed that MobMN199 binds Mn^{2+} with high affinity and one-to-one stoichiometry. The equilibrium constant (K_b) for the complex formation was 2.3 (±0.4) × $10^6\,M^{-1}$ and the enthalpy change (ΔH_b) −27.3 ± 0.3 kcal mol^{-1} (average of three experiments). These results evidenced that binding of Mn^{2+} to MobMN199 was enthalpically driven since the entropy change ($\Delta S_b = -65.2 \pm 0.7$ cal mol^{-1} K^{-1}) was largely unfavourable. The high affinity of Mn^{2+} for MobMN199 is consistent with the strong stabilization observed in the CD profiles at high cation concentrations (Figure 4). Further, the high values calculated for the enthalpic and entropic contributions indicate the existence of significant conformational rearrangements in the structure of MobMN199 upon Mn^{2+} binding. In contrast, no evidence of Mg^{2+} binding to MobMN199 was found neither from direct binding assays nor from the protein titration with Mn^{2+} in the presence of 10 mM Mg^{2+} (metal competition for the same site should have decreased the apparent affinity of MobMN199 for Mn^{2+}).

The effect of metal concentration on MobMN199 nicking-activity

MobM relaxation activity, measured by conversion of FI to FII forms, was previously tested in presence of different metal ions, being Mn^{2+} and Mg^{2+} the more efficient (19). Here we analysed the effect of Mn^{2+} and Mg^{2+} dosage on the activity of MobMN199, while keeping protein–DNA ratio (250 and 8 nM, respectively) and reaction conditions fixed. As shown in Figure 7, the nicking activity of MobMN199 strongly depended on the divalent cation concentration. Relaxed plasmid forms were not observed in the presence of EDTA (10 mM) or in the cation-free control. Maximum activity was found above 8 mM of divalent cation, with conversion levels to FII forms of 46 or 62% in the presence of saturating concentrations of $MgCl_2$ or $MnCl_2$, respectively. Interestingly, this difference in activity was also observed at 150 µM, a cation concentration high enough to provide full saturation of the high-affinity site of Mn^{2+} according to ITC data. Increase in MobMN199 activity with Mg^{2+} can be reasonably described assuming a single class of binding site with an apparent affinity of 1.8 mM (Figure 7c). For Mn^{2+}, however, a first increase accounting for ~15% FII

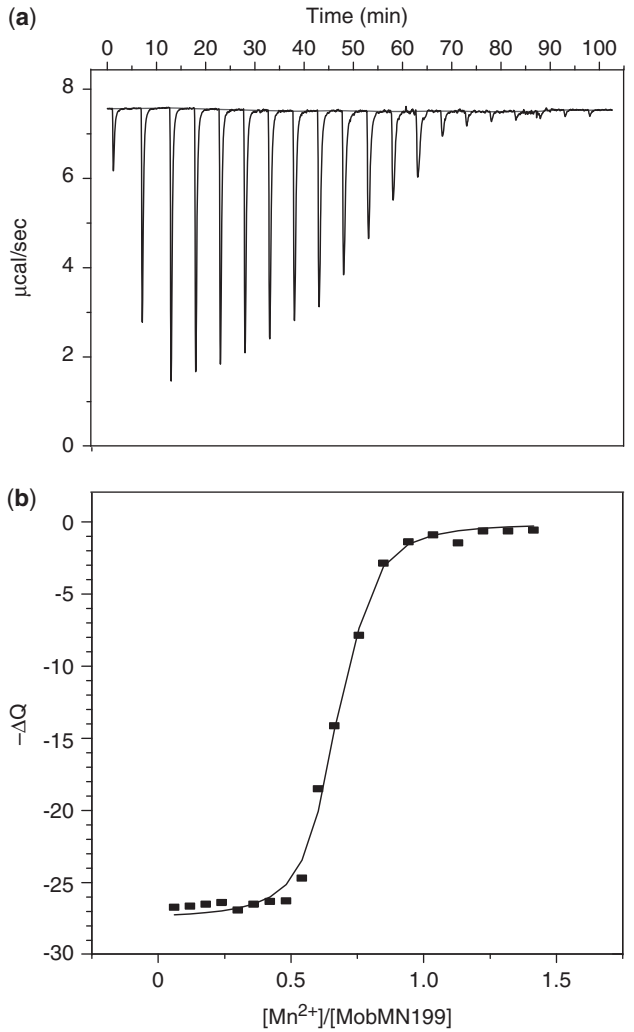

Figure 6. ITC binding analysis of Mn^{2+} by MobMN199. Raw data (top) for the injection of 1.5 mM $MnCl_2$ into a solution of MobMN199 (75 µM) and integrated heats of injection (bottom) are shown. The solid line shows the best data fit assuming a K_b of 2.3 $(\pm 0.4) \times 10^6\,M^{-1}$ and a ΔH_b, of -27.3 ± 0.3 kcal mol^{-1}.

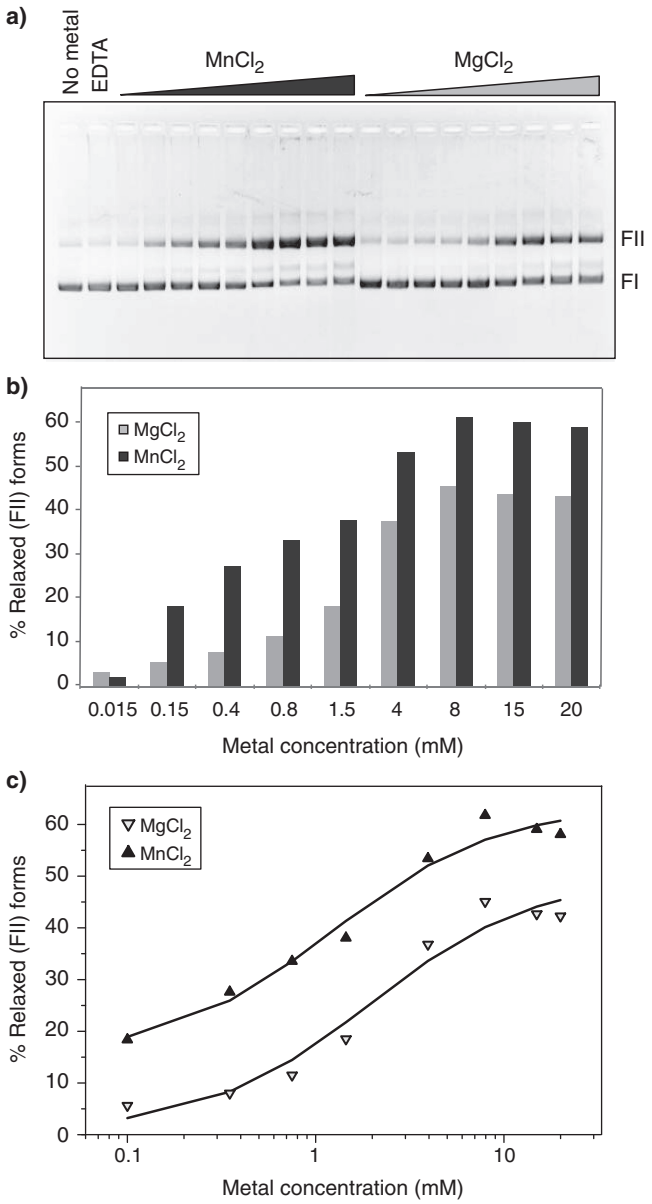

Figure 7. DNA nicking by the MobMN199 relaxase in the presence of different metal concentrations. (**a**) Supercoiled pMV158 DNA (8 nM) was incubated with MobMN199 (250 nM) in the presence of different concentrations of $MgCl_2$ or $MnCl_2$ (0.015, 0.2, 0.4, 0.8, 1.5, 4, 8, 15 and 20 mM) at 30°C for 20 min. Samples were analysed as indicated in Figure 1d. (**b**) Histogram comparing the percentage of FII plasmid forms generated by MobMN199 nicking activity in presence of $MgCl_2$ or $MnCl_2$. (**c**) Best fit of nicking activity data as function of metal ion concentration assuming a single set of metal ion-binding sites.

forms, followed by a further increase of ~48% at higher cation concentrations, was required to fit well the experimental data (Figure 7c). These results indicate that MobMN199 may contain two or more different classes of Mn^{2+} binding sites, at least in the presence of DNA, and that full nicking activity would be observed when the high and low affinity sites become saturated. Finally, based on this and on previously reported results (19), we can establish that the hierarchy of preference for cation usage by MobM is: $Mn^{2+} > Mg^{2+} > Ca^{2+} > Zn^{2+} \geq Ba^{2+}$.

MobMN199 interactions with ssDNA

The *oriT* of pMV158 was proposed to be included within a DNA region that contains IR1 and IR2 which encompassed the MobM-mediated nick site (located between coordinates 3591 and 3592) (20). A closer inspection of the sequence allowed us to find a third 31-bp IR (IR3) that includes IR1 plus 5 and 8 bases up- and downstream, respectively (Figure 8a). To reveal the requirements of the DNA target for recognition by MobMN199, we designed a set of Cy5-labelled oligonucleotides that contained part or all of the *oriT* sequence (Figure 8a). EMSA analysis using 2 nM of DNA showed that MobMN199 recognized specifically the *oriT* sequence, since it generated single complexes with the IR3-Cy5 and ORIT-Cy5 oligonucleotides (Figure 8b and c, respectively). However, MobMN199 did not bind to IR2-Cy5,

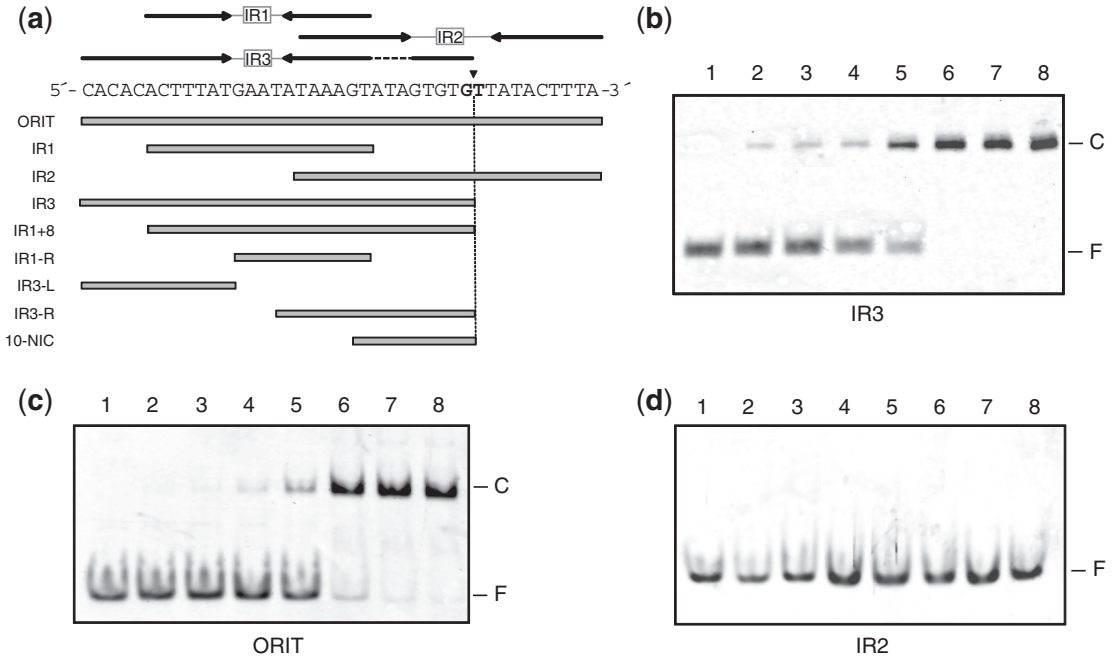

Figure 8. Interactions between MobMN199 and ss-oligonucleotides harbouring regions of the pMV158-*oriT*. (**a**) DNA sequence of the *oriT*, indicating the three inverted repeats (top) and the oligonucleotides used for affinity and competition analyses (bottom). The *nic* site is depicted by a vertical arrowhead. (**b–d**) MobMN199 DNA-binding measured by EMSA; the protein was incubated with Cy5-labelled DNA fragments containing the IR3 (b), the entire *oriT* (c) or the IR2 (d) sequences. MobMN199 concentrations were 0, 5, 10, 20, 40, 80, 160 and 320 nM from lane 1 to 8, respectively. Positions of the free (F) DNA and of the MobMN199–DNA complexes (C) are indicated.

even at high protein concentration (Figure 8d). After quantification of the bound DNA fraction, it was possible to estimate the dissociation constants (K_d) of MobMN199 as 60 ± 7 and 58 ± 6 nM for IR3 and ORIT oligonucleotides, respectively. These results indicate that the region encompassing IR1/3 was able to bind MobMN199 with high affinity. However, loss of the 5′-region of the *oriT* sequence (represented by oligonucleotide IR2) resulted in, at least, a 5-fold decrease in binding affinity ($K_d > 320$ nM). We also analysed the stoichiometry of MobMN199 binding to IR3 oligonucleotide. Graphic representation of the percentage of bound DNA showed that saturation was reached at an approximately 2:1 molar ratio of MobMN199:DNA (Supplementary Figure S2), which suggested the presence of two monomers of MobMN199 per DNA molecule in the complex. The same result was obtained with the ORIT oligonucleotide (data not shown).

The minimal *oriT* sequence includes IR1 hairpin

Competition binding assays between IR3-Cy5 (2 nM) and different amounts of the same unlabelled DNA (Figure 9a) or the ORIT oligonucleotide (Figure 9b) were performed. The results obtained at a fixed MobMN199 concentration (80 nM) showed a comparable competition ability of both oligonucleotides. This indicated that the recognition sites of MobMN199 for oligonucleotides IR3 and ORIT were equivalent. Thus, the minimal *oriT* region able to bind MobMN199 with high affinity could be located within the IR3 sequence. To test this hypothesis, new competition experiments were done using DNA fragments shorter than IR3. The results showed that a DNA including the IR1 hairpin sequence plus 8 nt downstream (IR1 + 8), just up to the nick site, was able to compete for binding of MobMN199 to IR3 with, at least, the same efficiencies than IR3 or ORIT (Figure 9c). However, other oligonucleotides harbouring only the IR1 sequence (IR1), the right-arm of IR3 (IR3-R), or 10 nt upstream the nick site (10-NIC), did not compete effectively with IR3-Cy5 for binding to MobMN199 at the concentrations employed (Figure 9d). The same behaviour was observed with oligonucleotides containing the left-arm of IR3 (IR3-L), right-arm of IR1 (IR1-R), or IR2 sequences (not shown).

To further examine the interactions between MobMN199 and IR1 + 8, the influence of DNA binding on the protein thermal stability was evaluated using DSC (Figure 5b) at low Mn^{2+}:MobMN199 ratio (ITC buffer). Addition of IR1 + 8 oligonucleotide at a protein:DNA molar ratio of 2:1 increased the T_m of the peak observed under similar conditions without DNA (Figure 5a) by >10°C (57.2 and 58.4°C at 13.3 and 40 μM MobMN199, respectively), and also induced a substantial increase in the enthalpy change (ΔH_D = 100 kcal/mol). A small shoulder was also visible at lower temperatures that might be due to DNA-free protein since no transitions were observed in the runs performed with IR1 + 8 in the absence of MobMN199 (not shown). The strong stabilization of the protein structure derived from the DNA–MobMN199 interaction was indicative of a tight complex formation. The dissociation rate constants of IR3 and IR1 + 8 oligonucleotides were also analysed. These measurements were

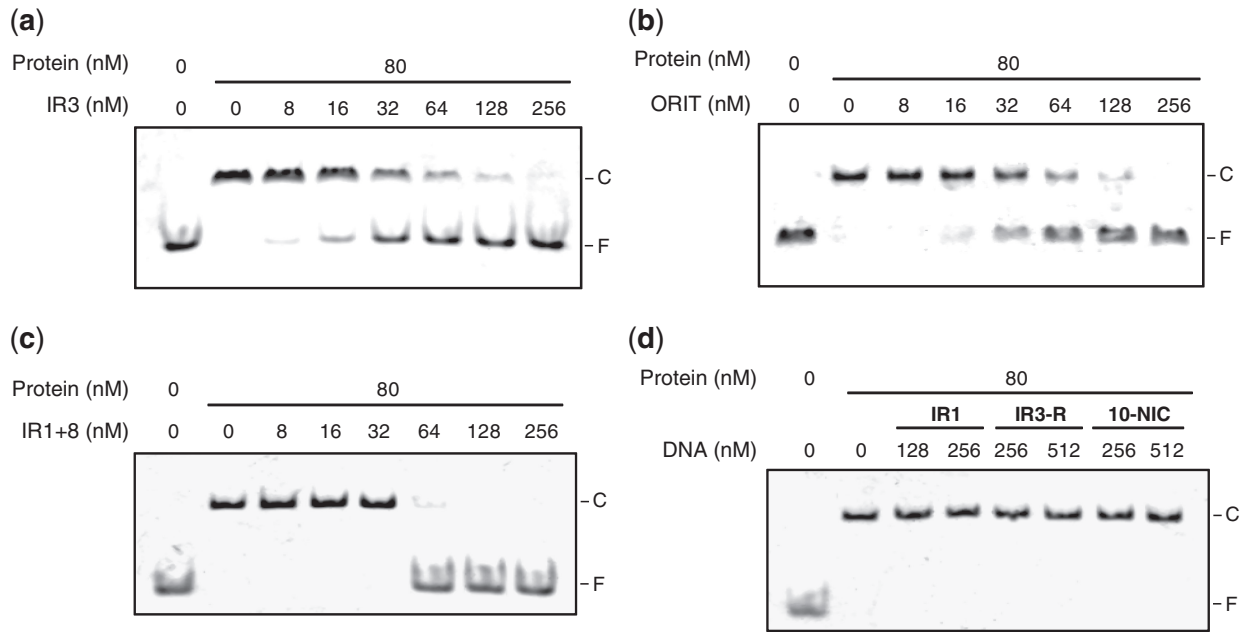

Figure 9. MobMN199 binding competitions between IR3-Cy5 and several unlabeled oligonucleotides. Different concentrations of competitor unlabeled IR3 (**a**), ORIT (**b**), IR1 + 8 (**c**), IR1, IR3 – R or NIC – 10 (**d**) oligonucleotides were mixed with 2 nM Cy5-labelled IR3. Then, purified MobMN199 protein (80 nM) was added to the reaction as indicated. Samples were incubated for 20 min at 24°C and loaded onto native PAA (10%) gels. Free (F) and complexed (C) DNA are indicated.

done by combining MobMN199 and labelled IR3-Cy5 oligonucleotide and then adding a 100-fold excess of IR3 or IR1 + 8 unlabelled oligonucleotides to prevent the re-association of labelled oligonucleotide after dissociation from MobMN199. The same behaviour was observed in both the cases, and the fit of the dissociation curves required two exponentials whose average rate constants were 0.030 min^{-1} and 0.001 min^{-1} (Supplementary Figure S3). All these results indicated that the minimal *oriT* target for MobMN199 binding on ssDNA is represented by IR1+8.

DISCUSSION

Here we present the first report on the location, at the N-terminal moiety, of the DNA-binding and DNA-nicking domain of MobM, the representative relaxase of the MOB_V family (24). We have separated the relaxase domain from the C-terminal moiety of the protein which, in turn, would harbour the regions involved in protein–protein interactions. Such interactions may include those with the coupling protein provided by either the host chromosome or the auxiliary plasmid participating in the transfer. Further, since MobMN199 was shown to be a monomer, rather than the dimer formed by the full-length protein (19), we propose that the C-terminal moiety would be also involved in MobM dimerization, which would be probably mediated by a putative leucine-zipper motif located between residues 317 and 338 (LENHSKSLEAKIECLESDNLQL). The truncated MobMN199 was unable to promote conjugal transfer of pMV158, as well as a MobM-derivative lacking the last 18 residues (results not shown), indicating the relevance of the C-terminal moiety for the *in vivo* function of MobM in pMV158 transfer.

Activity and stability of protein MobMN199

Spectroscopic and functional results evidenced the strong stabilization of MobMN199 structure provided by Mn^{2+} binding, which correlates with the high affinity of the cation for MobMN199 measured by ITC. The equilibrium constant ($2.3 \pm 0.3 \times 10^6\ M^{-1}$) was comparable to Mn^{2+} affinities for the minMobA (the relaxase domain of MobA; 186 residues) and TraI_F relaxases (K_b of 5×10^6 and $2 \times 10^6\ M^{-1}$, respectively) (48,49), and demonstrated that MobM exhibits high affinity binding for Mn^{2+} ions. Based on previous results obtained with the protein TraI_F (50), this site most likely corresponds to the 3H-motif of MobM (Figure 1a). Interestingly, despite its high binding affinity for Mn^{2+}, the metal ion concentration required for MobM optimal activity was >8 mM. This observation indicated that MobM protein may require the uptake of additional cations for an efficient DNA nicking activity than just the one bound to the active centre. In the case of the relaxase domain of minMobA, crystallographic and biophysical studies revealed that, apart from the active centre, there were two more Mn^{2+} binding sites of lower affinities ($K_b = 2.5 \times 10^4$ and $2.2 \times 10^4\ M^{-1}$) (22,49). Besides, variation of minMobA activity with cation concentration also supports the notion that saturation of metal ion low-affinity sites was required to reach the full activity (49). These observations indicate that this feature might be shared by other relaxases. Thus, cation binding might

help to organize the active site of MobMN199 and to position the DNA substrate (i.e. the scissile phosphate bond) for cleavage. Although the presence of multiple metal ions associating to several minMobA regions could have a protective effect, the stabilization of this protein against thermal denaturation at 1 mM Mn^{2+} was significantly lower than the one induced in MobMN199 under similar conditions. Irreversible processes accompanying thermal denaturation of minMobA might account for this unexpected observation. Whether protein stabilization reflects local changes or it extends to protein regions different from the metal binding site remains to be determined. Indeed, Mn^{2+} binding could provide a scaffold to the protein structure by stabilizing the 3H-motif and their coordination spheres, and compensate electrostatic charges on the protein surface. The magnitude of the enthalpy change together with the unfavourable entropy change accompanying the formation of the Mn^{2+}:MobMN199 complex also suggest some structural rearrangement upon Mn^{2+} coordination. As have been seen in several TrwC crystal structures, metal binding may cause some rearrangements in the protein conformation, specifically in the position of the catalytic tyrosine (51). Further, the failure of 15 mM Mg^{2+} to increase the thermal stability of MobMN199 may reflect a reduced affinity of this cation for MobMN199, at least in the absence of the DNA substrate, as was also observed by ITC analysis. The same behaviour has been reported for the minMobA relaxase that exhibited a slightly higher affinity for Mn^{2+} than for Mg^{2+} in the presence of DNA (49).

Spectroscopic analyses also showed that the temperature-induced changes in MobMN199 structure were partially reversible. The altered features of heated samples after being cooled down, relative to the native protein, could denote either: (i) the presence of a certain population of irreversibly denatured forms, or (ii) an incomplete recovery of the native structure. Indeed, the presence of Mg^{2+} or Mn^{2+} during heating and refolding seemed to facilitate the recovery of the closing activity and, therefore, the ability of MobMN199 to recuperate the full native structure, without changing significantly the nicking capacity of refolded molecules. Thermal denaturation of the TrwC relaxase domain showed that its α-helical core was resistant to temperature and responsible for the structural stabilization observed upon fast-heating thermal shock, whereas an outer layer of β-sheet and unordered structures unfolded and aggregated under slow heating (52). The combination of a compact core and a flexible outer layer could be related to the structural requirements of DNA–protein binding. In our case, MobMN199 retained its nicking/closing activity on supercoiled DNA after thermal denaturation-renaturation, provided that Mn^{2+} or Mg^{2+} was present, although protein denaturation seemed also to take place in several steps. This could be relevant for pMV158 transfer if we assume the currently accepted model in which the relaxase–DNA complex would be pumped into the recipient cell through a type-4 secretion system, which would require the protein to be unfolded (53,54).

Interactions of MobMN199 with DNA

Employment of fluorophore-labelled oligonucleotides (43) allowed us to study the interactions between MobMN199 and the *oriT* sequence in single-strand conformation. The *oriT* structure of pMV158 is different from the other well-known transfer systems because it exhibits three IRs instead of one. Recognition of *oriT* by MobMN199 was specific and the minimal *oriT* region defined here was constituted by the IR + 8 oligonucleotide (Figure 8). Similarly to other transfer systems, ssDNA substrates lacking the IR1 left arm of pMV158-*oriT* (represented by IR2, IR1-R, IR3-R and 10-NIC oligonucleotides; Figure 8a) showed very low affinities for MobMN199. In the case of TraI_F and TrwC, *in vitro* binding assays indicated that these proteins recognized their cognate *oriT*-containing oligonucleotides with higher affinities when they included a 5′-segment corresponding to an IR (7,25). The crystal structure of the TrwC relaxase domain bound to its cognate DNA showed that the IR generates a hairpin, which is involved in the strand-transfer reaction during the termination of conjugation (7,54). A recent report has corroborated this finding, showing that there are two distinguishable recognition-binding and cleavage-sites for TrwC, both required for efficient conjugation of R388 (28). Furthermore, the relaxase TraI_F could bind with high affinity to the same or similar DNA sequences in two different conformations (25). The two dissociation rate-constants observed in the kinetic analysis performed here suggest that there might be two different modes for the binding of *oriT*-containing oligonucleotides (IR3) to the MobMN199 protein. Furthermore, our results demonstrated that the average protein:IR3 stoichiometry was 2:1 as experimentally determined using EMSA. We propose that this may correlate with the dimeric nature of the native MobM protein (19), where each monomer could recognize two sites in the *oriT* during the plasmid transfer. Although the role of IR2 is still unknown, conservation of the *oriT* sequence among the MOB_V plasmid family (not shown) suggests that any one of the three IRs could be involved in the Mob-recognition of the *oriT* at the initiation of relaxosome formation in the donor cell and/or termination reaction to close the T-strand, in the recipient cell.

Relevance of Mn^{2+} in pMV158 and related plasmids

The only available information on metal ion recognition in MOB_V family is represented by Mob_pBBR1 from *Bordetella bronchiseptica* (55) and BmpH_Tn*5520* from *Bacteroides fragilis* (56) systems; both are active with Mg^{2+}. It would be interesting to know whether the selection of the cation reflects a preference for proteins of the MOB_V family, or a preference in Mn^{2+} utilization by *S. pneumoniae*. In this sense, it is worth pointing out that the second nucleotidyl-transferase encoded by pMV158, the RepB initiator of RCR, also required Mn^{2+} for optimal activity (57). Furthermore, this cation was present in the active pocket of the protein as observed in the three-dimensional (3D) structure of RepB (47). The discovery of the pneumococcal *mntE* Mn^{2+} efflux system

as involved in pathogenesis and invasive response of this bacterium (58), supports the relevance of this cation *in vivo* and, perhaps, in transactions involved in horizontal transfer of genetic material (conjugation and transformation being the two most relevant processes in *S. pneumoniae*). Nevertheless, further experiments, including the solution of the structure of the MobM protein bound to its DNA target, will allow us a deeper biochemical and structural characterization of the MOB_V family of relaxases, as well as a better understanding of the mechanisms involved in transfer of the pMV158 promiscuous replicon.

SUPPLEMENTARY DATA

Supplementary Data are available at NAR Online.

ACKNOWLEDGEMENTS

Thanks are due to Dr Jose A. Ruiz-Masó for his help on CD assays, Lorena Rodríguez-González for her assistance in protein purification, Dr Douglas V. Laurents for linguistic revision and Victoria López-Moyano for her help in calorimetric experiments. Discussions with members of Espinosa's lab are also acknowledged.

FUNDING

Funding for open access charge: Spanish Ministry of Science and Innovation [grants CSD2008-00013, INTERMODS to M.E.; BFU2008-02372/BMC, PRODNA to M.C.; BFU2009-10052 and CIBERES (an initiative of the Carlos III Spanish Health Institute) to M.M.]; European Union (grant EU-CP223111, CAREPNEUMO to M.E.); National Institutes of Health (grant GM61017 to J.F.S.); The Carlos III Spanish Health Institute, fellowship BF03/00529 (to F.L.-D.).

Conflict of interest statement. None declared.

REFERENCES

1. Baquero,F. (2004) From pieces to patterns: evolutionary engineering in bacterial pathogens. *Nature Rev. Microbiol.*, **2**, 510–518.
2. Espinosa,M., Cohen,S., Couturier,M., del Solar,G., Díaz-Orejas,R., Giraldo,R., Janniére,L., Miller,C., Osborn,M. and Thomas,C.M. (2000) Plasmid replication and copy number control. In Thomas,C.M. (ed.), *The Horizontal Gene Pool*. Harwood Academic Publishers, Amsterdam, pp. 1–47.
3. Mandell,L.A., Wunderink,R.G., Anzueto,A., Bartlett,J.G., Campbell,G.D., Dean,N.C., Dowell,S.F., File,T.M. Jr, Musher,D.M., Niederman,M.S. *et al.* (2007) Infectious Diseases Society of America/American Thoracic Society consensus guidelines on the management of community-acquired pneumonia in adults. *Clin. Infect. Dis.*, **44 (Suppl. 2)**, S27–S72.
4. Woodbury,R.L., Klammer,K.A., Xiong,Y., Bailiff,T., Glennen,A., Bartkus,J.M., Lynfield,R., Van Beneden,C., Beall,B.W. and for the Active Bacterial Core Surveillance Team. (2008) Plasmid-borne *erm*(T) from invasive, macrolide-resistant *Streptococcus pyogenes* strains. *Antimicrob. Agents Chemother.*, **52**, 1140–1143.
5. Lanka,E. and Wilkins,B.M. (1995) DNA processing reactions in bacterial conjugation. *Annu. Rev. Biochem.*, **64**, 141–169.
6. Datta,S., Larkin,C. and Schildbach,J.F. (2003) Structural insights into single-stranded DNA binding and cleavage by F factor TraI. *Structure*, **11**, 1369–1379.
7. Guasch,A., Lucas,M., Moncalián,G., Cabezas,M., Pérez-Luque,R., Gomis-Rüth,F.X., de la Cruz,F. and Coll,M. (2003) Recognition and processing of the origin of transfer DNA by conjugative relaxase TrwC. *Nat. Struct. Biol.*, **10**, 1002–1010.
8. de la Cruz,F., Frost,L.S., Meyer,R.J. and Zechner,E.L. (2010) Conjugative DNA metabolism in Gram-negative bacteria. *FEMS Microbiol. Rev.*, **34**, 18–40.
9. Llosa,M., Gomis-Rüth,F.X., Coll,M. and de la Cruz,F. (2002) Bacterial conjugation: a two-step mechanism for DNA transport. *Mol. Microbiol.*, **45**, 1–8.
10. Novick,R.P. (1998) Contrasting lifestyles of rolling-circle phages and plasmids. *TIBS*, **23**, 434–438.
11. Lorenzo-Díaz,F. and Espinosa,M. (2009) Lagging strand DNA replication origins are required for conjugal transfer of the promiscuous plasmid pMV158. *J. Bacteriol.*, **191**, 720–727.
12. Parker,C. and Meyer,R. (2005) Mechanisms of strand replacement synthesis for plasmid DNA transferred by conjugation. *J. Bacteriol.*, **187**, 3400–3406.
13. Francia,M.V., Varsaki,A., Garcillán-Barcia,M.P., Latorre,A., Drainas,C. and de la Cruz,F. (2004) A classification scheme for mobilization regions of bacterial plasmids. *FEMS Microbiol. Revi.*, **28**, 79–100.
14. Grohmann,E., Muth,G. and Espinosa,M. (2003) Conjugative plasmid transfer in Gram-positive bacteria. *Microbiol. Mol. Biol. Rev.*, **67**, 277–301.
15. Kopec,J., Bergmann,A., Fritz,G., Grohmann,E. and Keller,W. (2005) TraA and its N-terminal relaxase domain of the Gram-positive plasmid pIP501 show specific *oriT* binding and behave as dimers in solution. *Biochem. J.*, **387**, 401–409.
16. Kurenbach,B., Kopec,J., Magdefrau,M., Andreas,K., Keller,W., Bohn,C., Abajy,M.Y. and Grohmann,E. (2006) The TraA relaxase autoregulates the putative type IV secretion-like system encoded by the broad-host-range *Streptococcus agalactiae* plasmid pIP501. *Microbiology*, **152**, 637–645.
17. Caryl,J.A., Smith,M.C.A. and Thomas,C.D. (2004) Reconstitution of a staphylococcal plasmid-protein relaxation complex *in vitro*. *J. Bacteriol.*, **186**, 3374–3383.
18. Caryl,J.A. and Thomas,C.D. (2006) Investigating the basis of substrate recognition in the pC221 relaxosome. *Mol. Microbiol.*, **60**, 1302–1318.
19. de Antonio,C., Farias,M.E., de Lacoba,M.G. and Espinosa,M. (2004) Features of the plasmid pMV158-encoded MobM, a protein involved in its mobilization. *J. Mol. Biol.*, **335**, 733–743.
20. Guzmán,L. and Espinosa,M. (1997) The mobilization protein, MobM, of the streptococcal plasmid pMV158 specifically cleaves supercoiled DNA at the plasmid *oriT*. *J. Mol. Biol.*, **266**, 688–702.
21. Ilyina,T. and Koonin,E. (1992) Conserved sequence motifs in the initiator proteins for rolling circle DNA replication encoded by diverse replicons from eubacteria, eukaryotes and archaebacteria. *Nucleic Acids Res.*, **20**, 3279–3285.
22. Monzingo,A.F., Ozburn,A., Xia,S., Meyer,R.J. and Robertus,J.D. (2007) The structure of the minimal relaxase domain of MobA at 2.1 Å resolution. *J. Mol. Biol.*, **366**, 165–178.
23. Nash,R.P., Habibi,S., Cheng,Y., Lujan,S.A. and Redinbo,M.R. (2010) The mechanism and control of DNA transfer by the conjugative relaxase of resistance plasmid pCU1. *Nucleic Acids Res.*, **38**, 5929–5943.
24. Garcillán-Barcia,M.P., Francia,M.V. and de la Cruz,F. (2009) The diversity of conjugative relaxases and its application in plasmid classification. *FEMS Microbiol. Rev.*, **33**, 657–687.
25. Williams,S.L. and Schildbach,J.F. (2006) Examination of an inverted repeat within the F factor origin of transfer: context dependence of F TraI relaxase DNA specificity. *Nucleic Acids Res.*, **34**, 426–435.
26. Hekman,K., Guja,K., Larkin,C. and Schildbach,J.F. (2008) An intrastrand three-DNA-base interaction is a key specificity determinant of F transfer initiation and of F TraI relaxase DNA recognition and cleavage. *Nucleic Acids Res.*, **36**, 4565–4572.

27. González-Pérez,B., Lucas,M., Cooke,L.A., Vyle,J.S., de la Cruz,F. and Moncalián,G. (2007) Analysis of DNA processing reactions in bacterial conjugation by using suicide oligonucleotides. *EMBO J.*, **26**, 3847–3857.
28. Lucas,M., González-Pérez,B., Cabezas,M., Moncalián,G., Rivas,G. and de la Cruz,F. (2010) Relaxase DNA binding and cleavage are two distinguishable steps in conjugative DNA processing that involve different sequence elements of the *nic* site. *J. Biol. Chem.*, **285**, 8918–8926.
29. Lacks,S., López,P., Greenberg,B. and Espinosa,M. (1986) Identification and analysis of genes for tetracycline resistance and replication functions in the broad-host-range plasmid pLS1. *J. Mol. Biol.*, **192**, 753–765.
30. del Solar,G., Díaz,R. and Espinosa,M. (1987) Replication of the streptococcal plasmid pMV158 and derivatives in cell-free extracts of *Escherichia coli*. *Mol. Gen. Genet.*, **206**, 428–435.
31. Laue,T.M., Shah,B.D., Ridgeway,T.M. and Pelletier,S.L. (1992) In Harding,S.E., Rowe,A. and Horton,J.C. (eds), *Analytical Ultracentrifugation in Biochemistry and Polymer Sciences*. Royal Society of Chemistry, Cambridge, pp. 90–125.
32. Schuck,P. and Rossmanith,P. (2000) Determination of the sedimentation coefficient distribution by least-squares boundary modeling. *Biopolymers*, **54**, 328–341.
33. van Holde,K.E. (1985) *Physical Biochemistry*, 2nd edn. Englewoods Cliffs, Prentice Hall.
34. Pessen,H. and Kumosinsky,T.F. (1985) Measurement of protein hydration by various techniques. *Meth. Enzymol.*, **117**, 219–255.
35. McGuffin,B.K. and Jones,D.T. (2000) The PSIPRED protein structure prediction server. *Bioinformatics*, **16**, 404–405.
36. Cole,C., Barber,J.D. and Barton,G.J. (2008) The Jpred 3 secondary structure prediction server. *Nucleic Acids Res.*, **36**, 197–201.
37. Adamczak,R., Porollo,A. and Meller,J. (2005) Combining prediction of secondary structure and solvent accessibility in proteins. *Proteins: Struct. Funct. Bioinformatics*, **59**, 467–475.
38. Combet,C., Blanchet,C., Geourjon,C. and Deléage,G. (2000) NPS@: network protein sequence analysis. *TIBS*, **25**, 147–150.
39. Rost,B., Yachdav,G. and Liu,J. (2004) The PredictProtein server. *Nucleic Acids Res.*, **32**, W321–W326.
40. van Stokkum,I.H.M., Spoelder,H.J.W., Bloemendal,M., van Grondelle,R. and Groen,F.C.A. (1990) Estimation of protein secondary structure and error analysis from CD spectra. *Anal. Biochem.*, **191**, 110–118.
41. Sreerama,N. and Woody,R.W. (2000) Estimation of protein secondary structure from circular dichroism spectra: Comparison of CONTIN, SELCON, and CDSSTR methods with an expanded reference set. *Anal. Biochem.*, **287**, 252–260.
42. Whitmore,L. and Wallace,B.A. (2004) DICHROWEB, an online server for protein secondary structure analyses from circular dichroism spectroscopic data. *Nucleic Acids Res.*, **32(web server issue)**, 668–673.
43. Anderson,B.J., Larkin,C., Guja,K. and Schildbach,J.F. (2008) Using fluorophore-labeled oligonucleotides to measure affinities of protein-DNA interactions. *Method. Enzymol.*, **450**, 253–272.
44. Llosa,M., Grandoso,G. and de la Cruz,F. (1995) Nicking activity of TrwC directed against the origin of transfer of the IncW plasmid R388. *J. Mol. Biol.*, **246**, 54–62.
45. Matson,S.W. and Morton,B.S. (1991) *Escherichia coli* DNA helicase I catalyzes a site- and strand-specific nicking reaction at the F plasmid *oriT*. *J. Biol. Chem.*, **266**, 16232–16237.
46. Pansegrau,W., Balzer,D., Kruft,V. and Lanka,E. (1990) *In vitro* assembly of relaxosomes at the transfer origin of plasmid RP4. *Proc. Natl Acad. Sci. USA*, **87**, 6555–6559.
47. Boer,D.R., Ruíz-Masó,J.A., López-Blanco,J.R., Blanco,A.G., Vives-Llàcer,M., Chacón,P., Usón,I., Gomis-Rüth,F.X., Espinosa,M., Llorca,O. *et al.* (2009) Plasmid replication initiator RepB forms a hexamer reminiscent of ring helicases and has mobile nuclease domains. *EMBO J.*, **28**, 1666–1678.
48. Larkin,C., Datta,S., Harley,M.J., Anderson,B.J., Ebie,A., Hargreaves,V. and Schildbach,J.F. (2005) Inter- and Intra-molecular determinants of the specificity of single-stranded DNA binding and cleavage by the F factor relaxase. *Structure*, **13**, 1533–1544.
49. Xia,S. and Robertus,J.D. (2009) Effect of divalent ions on the minimal relaxase domain of MobA. *Arch. Biochem. Biophys.*, **488**, 42–47.
50. Larkin,C., Haft,R.J.F., Harley,M.J., Traxler,B. and Schildbach,J.F. (2007) Roles of active site residues and the HUH motif of the F plasmid TraI relaxase. *J. Biol. Chem.*, **282**, 33707–33713.
51. Boer,R., Russi,S., Guasch,A., Lucas,M., Blanco,A.G., Perez-Luque,R., Coll,M. and de la Cruz,F. (2006) Unveiling the molecular mechanism of a conjugative relaxase: The structure of TrwC complexed with a 27-mer DNA comprising the recognition hairpin and the cleavage site. *J. Mol. Biol.*, **358**, 857–869.
52. Arrondo,J.L.R., Echabe,I., Iloro,I., Hernando,M.A., de la Cruz,F. and Goñi,F.M. (2003) A bacterial TrwC relaxase domain contains a thermally stable α-helical core. *J. Bacteriol.*, **185**, 4226–4232.
53. Draper,O., Cesar,C.E., Machon,C., de la Cruz,F. and Llosa,M. (2005) Site-specific recombinase and integrase activities of a conjugative relaxase in recipient cells. *PNAS*, **102**, 16385–16390.
54. Garcillán-Barcia,M.P., Jurado,P., González-Pérez,B., Moncalián,G., Fernández,L.A. and de la Cruz,F. (2007) Conjugative transfer can be inhibited by blocking relaxase activity within recipient cells with intrabodies. *Mol. Microbiol.*, **63**, 404–416.
55. Szpirer,C.Y., Faelen,M. and Couturier,M. (2001) Mobilization function of the pBHR1 plasmid, a derivative of the broad-host-range plasmid pBBR1. *J. Bacteriol.*, **183**, 2101–2110.
56. Vedantam,G., Knopf,S. and Hecht,D.W. (2006) *Bacteroides fragilis* mobilizable transposon Tn*5520* requires a 71 base pair origin of transfer sequence and a single mobilization protein for relaxosome formation during conjugation. *Mol. Microbiol.*, **59**, 288–300.
57. de la Campa,A.G., del Solar,G. and Espinosa,M. (1990) Initiation of replication of plasmid pLS1. The initiator protein RepB acts on two distant DNA regions. *J. Mol. Biol.*, **213**, 247–262.
58. Rosch,J.W., Gao,G., Ridout,G., Wang,Y.-D. and Tuomanen,E. (2009) Role of the manganese efflux system *mntE* for signalling and pathogenesis in *Streptococcus pneumoniae*. *Mol. Microbiol.*, **72**, 12–25.